Journal of Materials Chemistry C

Accepted Manuscript

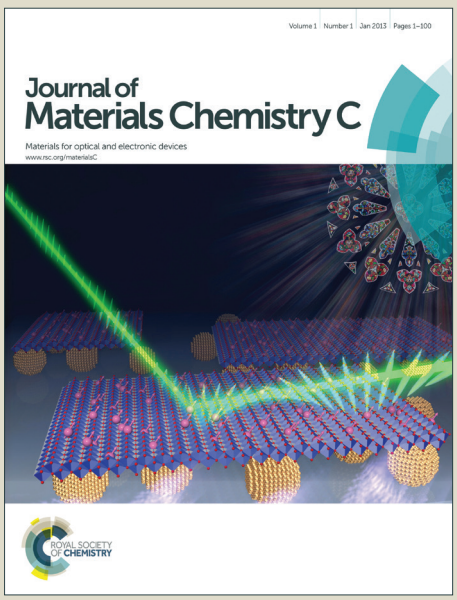

ROYAL SOCIETY OF CHEMISTRY

www.rsc.org/materialsC

Submitted to **Journal of Materials Chemistry C**

High-stable and Stretchable Graphene-Polymer processed Silver Nanowires Hybrid Electrodes for Flexible Displays

Qi Zhang,[a] Yanfei Di,[a] Chad M. Huard,[b] L. Jay Guo,[b] Jie Wei,[a] Jinbao Guo[a*]

[a]College of Materials Science and Engineering, Beijing University of Chemical Technology, Beijing 100029, P. R. China

[b]Department of Electrical Engineering and Computer Science, University of Michigan, Ann Arbor, Michigan 48109

*To whom correspondence should be addressed.

guojb@mail.buct.edu.cn

Abstract:

A new kind of high-stable, transparent and flexible hybrid electrodes has been developed by integrating the encapsulation of silver nanowires (AgNWs) network by polyvinyl alcohol (PVA) with a single-layer graphene on a flexible substrate. Compared with commercial indium tin oxide (ITO) film and the pristine AgNWs-graphene hybrid film, this hybrid electrode formulations were found to exhibit excellent optical and electrical properties (84.0% at 550 nm R_S=14.1Ω/□). Moreover, PVA encapsulated-AgNWs/graphene hybrid electrode on a flexible substrate shows superior mechanical flexibility, reliability and long-term stability due to the multi-functional effects of the PVA as the encapsulation layer. Finally, we employ this hybrid electrode to construct a flexible cholesteric liquid crystals (Ch-LCs) device, where the PVA layer in hybrid formation could be used as orientation layer. This Ch-LCs device exhibits an impressive electrical-optical performance, demonstrating its potential as a transparent and stretchable electrode platform for flexible optoelectronics.

.

Introduction

Flexible optoelectronics devices on plastic substrates, such as organic light-emitting device (OLED), liquid crystal display (LCD) and organic solar cells (OSCs), have gained much attention during these years. However, the development of these flexible devices is still limited by the suitable electrode materials. Indium tin oxide (ITO) is the most commonly used transparent electrode in electric and optical devices, but it is not suitable for flexible devices due to its brittleness nature.[1] Therefore, some conducting materials as an alternative to ITO including conducting polymers, carbon nanotubes (CNTs), graphene, metal grids, and metallic nanowires have been investigated extensively.[2-12]

Among these materials, single-layer and multi-layer graphene have attracted great interest as a transparent conductor because of its high chemical and thermal stability, high stretchability, high optical transparency and low contact resistance.[13,14] Additionally, chemical vapor deposition (CVD) of hydro-carbon gases on metal surfaces allows scaling graphene films to large sizes that can be transferred onto arbitrary substrates.[15-17] For example, we recently employ a CVD-grown single-layer graphene electrode together with a metal–dielectric–metal sandwiched Fabry–Perot (F–P) cavity film to build an ITO-free and more compact and color LC device.[18] However, Large-area CVD-grown graphene is a polycrystalline material with topological defects such as dislocations and grain boundaries which may form of highly resistive grain boundaries, thereby leading to the carriers being trapped periodically in domains. Additionally, a higher electrical resistivity than theoretical

values of the graphene can arise from other defects, such as ripples point defects, wrinkles, tears and cracks, which also influence the charge carriers resulting in decreased ballistic transport path length and carrier mobility.[19] To lower these impacts, some graphene-based hybrid structures have been investigated by employing conducting polymer and metal nanowires (NWs).[19-25]

Among metal NWs, silver NWs (AgNWs) has been widely investigated due to facile fabrication, high conductivity and mechanical flexibility.[26-31] Kholmanov et al. demonstrated that line defects and line disruptions in transferred CVD-grown polycrystalline graphene films can be eliminated by combining of graphene with AgNWs.[19] Liu et al. reported a transparent and flexible hybrid electrode by coating AgNWs network with graphene film on a PET substrate, where the resultant hybrid film has a lower surface roughness, high DC to optical conductivity ratios and excellent bending property.[22] Lee et al. developed a AgNWs-graphene hybrid electrode by dry-transferring a CVD-grown monolayer graphene onto a AgNWs network, which shows highly enhanced thermal oxidation and chemical stabilities due to the gas-barrier effect of the graphene layer.[23] However, although AgNWs could be conductive to decreasing the sheet resistance (R_S) of the CVD-grown graphene electrodes, there are still some issues need to address. The limited point for the hybrid structure, where CVD-grown monolayer graphene is on top of AgNWs network, is that complicated, *in situ* graphene processing flow after deposition of the surface of AgNWs, which may destroy the AgNWs network and induce surface roughness during the removal of the polymer layer.[19,22] Additionally, the hybrid structure of the

AgNWs network on graphene film, the long-term stability tends to be greatly decreased due to the easy oxidation of the AgNWs in air.[24] Therefore, it is necessary to develop new hybrid electrode formulation based on graphene and AgNWs.

In this study, we develop a sandwich-structure hybrid electrode, in which the polyvinyl alcohol (PVA)-encapsulated AgNWs network is on top of the single-layer graphene. As mentioned above, the AgNWs are easily oxidized when they are exposed to air and water, leading to a sharp increase of R_S and haziness of the AgNWs electrode. Herein, among the alternative polymers,[27,30,32-34] we choose PVA as the top layer of this hybrid electrode film based on the following points. First, it can help to achieve more intimate contact between the graphene and AgNWs as well as at the junctions between AgNWs; Second, it increases the adhesion between the AgNWs and CVD graphene, thereby improving mechanical robustness against adhesion, friction, and bending; Third, PVA layer can be used as a protective layer to inhibit AgNWs oxidation; Finally, when we use this hybrid electrodes to build a flexible cholesteric LCs (Ch-LCs) device, PVA layer could also be used as alignment film to induce the planar orientation of LC molecules. This work opens up a new way to optimizing the performance of AgNWs-graphene hybrid electrodes by introducing polymers and other related materials.

Experimental section

Materials

AgNWs ink was purchased from Zhejiang Kechuang Advanced Materials Co., Ltd. (Average size: Ave. Diameter D=35~45 nm, Ave. Length L=10~20 um). Nematic-LC,

SLC-1717 (20 ^{o}C, 589 nm, Δn=0.201), was purchased from Shijiazhuang Chengzhi Yonghua Display Materials Co. Ltd. Photo-switchable chiral dopant, (S)-BnAzoDe-(S)-Oy was synthesized as described in our previous paper.[35] All other materials, solvents and reagents were obtained from commercial sources and used without further purification.

Preparation of single layer graphene

The detail description how to synthesis a single layer graphene can be obtained in our previous paper.[18] The following is a brief description. The copper foil was placed in a CVD system with a quartz tube and heated to 1000 °C with H_2 and Ar. The foil was annealed for 30 minutes at this temperature，then CH_4 is flowed with H_2 and Ar. After CVD growth, the Cu foil was coated with a layer of 950PMMA A9, and immersed into ferric chloride copper etchant solution in order to etch away the Cu foil. When Cu was completely etched away, the graphene sheets with PMMA were transferred onto a PET substrate, unless otherwise stated. Then, the PMMA coating is removed with acetone and the substrate is rinsed with deionized water several times.

Preparation of hybrid electrodes

First, we spray-coated AgNWs onto single-layer graphene, AgNWs ink was re-dispersed in methyl alcohol to form a AgNWs/methyl alcohol (MeOH) solution (0.1mg/ml). The temperature of the heated plate was set to 140 ^{o}C before spraying. The air-brush of the spray gun was set with a spraying distance of ~3 cm from the surface of the CVD graphene transferred on glass or PET substrate. We can control the deposition density of AgNWs by adjusting the volume of the solution. After

spraying, the AgNWs-graphene film was heated at 140 °C for 30min. After the hybrid film cooled down to room temperature, an aqueous solution of PVA-124 (3 wt%) was spin-coated over the hybrid film. The thickness of the AgNWs/PVA film can be changed by controlling the rotation speed, which varies from 2500 to 4000 rpm in different states. Then, the hybrid film was dried at 80 ^{o}C for 2 hours.

Fabrication of Ch-LCs Devices

The Ch-LCs mixture was prepared by weighing appropriate amount of host LCs and the chiral dopant into a vial, and we blend them with addition of a few drops of dichloromethane. After evaporation of the solvent under reduced pressure, the Ch-LCs mixture was prepared. Our mixture contains SLC-1717 (96.5 wt%) and photoresponsive chiral dopant of (S)-BnAzoDe-(S)-Oy (3.5wt%). Then, the Ch-LCs mixture was laminated between two PVA-encapsulated AgNWs-graphene hybrid films on PET substrates, in which PVA layer was mechanically rubbed as the alignment film. Herein, polystyrene beads with 6 μm thickness were used as the cell spacers. After that, a "BUCT" pattern was addressed on the LC cell by using UV light with a negative photomask placed on the top of the cell. The color of each addressed pattern letter was controlled by the exposure time of UV light at a constant UV light intensity (2mW/cm^2). Finally, the formed LC device was driven by the electric field and the patterned image can be completely erased and reappeared at different certain voltage.

Measurements

Sheet resistance (R_S) was measured using a SB118 DC voltage and current source in

conjunction with a Jandel 4 point probe unit, and values reported are taken to be the average of a minimum of 6-8 measurements from random parts of the substrate unless otherwise stated. UV-Vis spectra were taken on a Hitachi U-3100 spectrophotometer operating in normal mode. The transmission data has been corrected for the PET substrate unless otherwise stated. Atomic force microscopy (AFM) was performed in tapping mode on Dimension 3100 from Veeco Instruments. Scanning electron microscopy (SEM) images were taken using a JSM-7410F high resolution microscope with an accelerating voltage of 3 kV. Samples on PET substrate have a thin layer of gold sputtered on top to assist with imaging. The formed device was driven using a signal generator named HT102V4 and purchased from Halation Technology Co. Ltd., Beijing, China.

Results and discussion

Figure 1a provides the schematic diagram of the fabrication of the PVA encapsulated AgNWs-graphene hybrid electrode films, and Figures 1b and 1c show a photograph of PVA encapsulated AgNWs-graphene hybrid electrode on a PET substrate and the corresponding curving exhibition of this hybrid formation, respectively. We note that, the red box on the background of “BUCT” is PVA encapsulated AgNWs-graphene hybrid electrode and the vicinity is PVA encapsulated AgNWs without a single-layer graphene. Herein, the optical transmittance of the PVA encapsulated AgNWs-graphene was a little reduced due to the absorbance of single-layer graphene in the visible spectrum (Supporting Information: Fig. S1 and Fig. S2). First, we fabricate a single-layer graphene on a flexible PET substrate by using a CVD process

as mentioned above, which includes CVD synthesis, coating of graphene with PMMA, copper etching, transferring and removing of the polymer layer, the fabrication process was detailedly described in our previous study and also the experimental section.[18] Raman spectrum as demonstrated in Figure 2a shows a feature similar to that of single-layer graphene: a 2D to G intensity ratio of >1 and a symmetric 2D band centered at 2643 cm^{-1} with a full width at half maximum of 39 cm^{-1}, indicating that the graphene film is single-layer dominant. Morphological images of the single-layer graphene were taken using AFM and SEM. Both the AFM (Figure 2b) and SEM (Figure 2c) show uniform and clean graphene sheets. In addition, some wrinkles could be observed in Figure 2b-c, which is one of essential features of the CVD-growth method for graphene fabrication. Figure 2d shows photographic image of a single-layer graphene on a flexible PET substrate. The R_S of single-layer graphene sample we fabricated is measured to be around 1000 Ω/□ by using four-point method.

Second, the AgNWs of MeOH (0.1mg/ml) solution was precipitated onto the single-layer graphene film by employing a spraying solution and the deposition density of AgNWs could be controlled by adjusting the volume of the solution. Here deposition densities of AgNWs increase from 30 mg/m^2 to 150 mg/m^2 in order to investigate the effects of AgNWs deposition density on the electric and optical performances of the hybrid films. After a 30 min annealing process at 140 ^oC, the hybrid films were cooled down to room temperature. Finally, PVA aqueous solution (3 wt%) was spin-coated over the hybrid films, then a hybrid transparent and flexible

conductive electrode on PET substrate was prepared, in which the AgNWs network encapsulated by a PVA layer was laminated onto a single-layer graphene film. We note that, this hybrid structure is different from that of the previous study, where the dried PVA matrix together with encapsulated AgNWs was peeled off the PET surface.[32] Herein, the thickness of the PVA layer was optimized by adjusting the spin rate and coating time in order to achieve a better electric and optical performance of hybrid conductors.

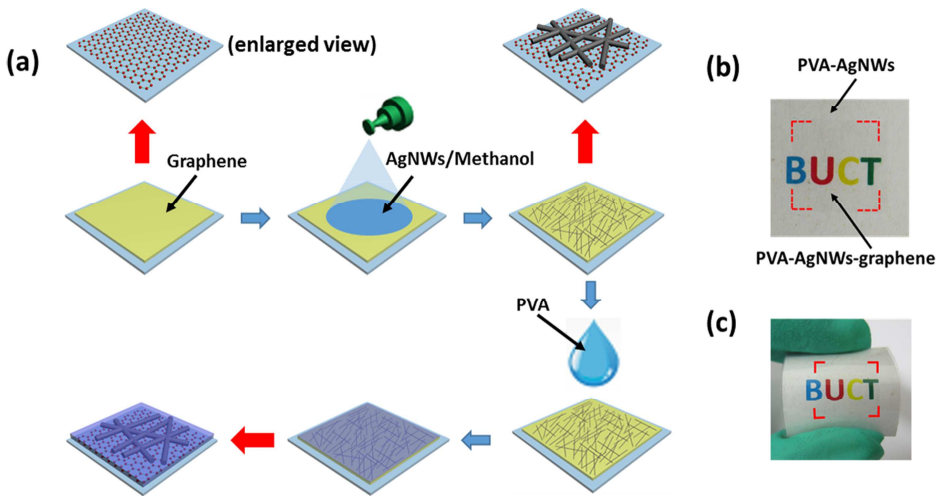

Fig. 1. (a): Schematic illustration of the fabrication procedure of PVA encapsulated AgNWs-graphene hybrid film; (b): A photograph of PVA encapsulated AgNWs-graphene hybrid electrode on a PET substrate and (c): A curving show of PVA encapsulated AgNWs-graphene hybrid electrode film on a PET substrate.

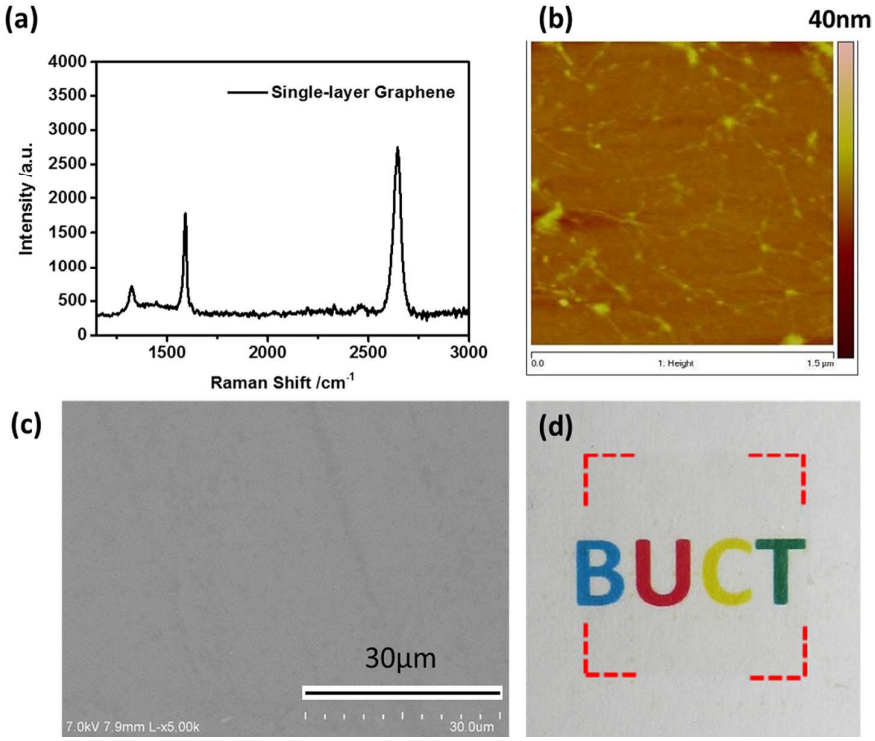

Fig. 2. (a): Raman spectrum of single-layer graphene, the spectrum was taken using transferred graphene on the glass surface; (b): AFM image of graphene on a glass substrate; (c): SEM image of the graphene on a glass substrate; (d): Photograph of graphene on PET substrate.

To estimate the electrical and optical performance of the novel hybrid TCE, we measured the R_S and optical transmittance of the novel hybrid TCEs. Figure 3 shows the R_S of the AgNWs/graphene hybrid films before and after uniform coating of PVA layer. Increasing the AgNWs deposition density resulted in obviously decreased R_S of the pristine AgNWs-graphene hybrid films. For example, by increasing the AgNWs deposition density from 30 to 150 mg/m^2, the R_S of the pristine AgNWs- graphene hybrid films decreased from 142.8 Ω/□ to 12.7 Ω/□ (curve 1). The result demonstrates that increasing the AgNWs deposition density is beneficial to the electrical

performance of the pristine AgNWs-graphene hybrid films. However, the decreasing amplitude of R_S starts to level off after the AgNWs deposition density reaches about 120mg/m^2. The improvement of R_S could be attributed to that the electron transport barrier of single-layer graphene is surrounded by the transport channels of AgNWs deposited on the top of graphene layer and vice verse.[24] Furthermore, by comparing

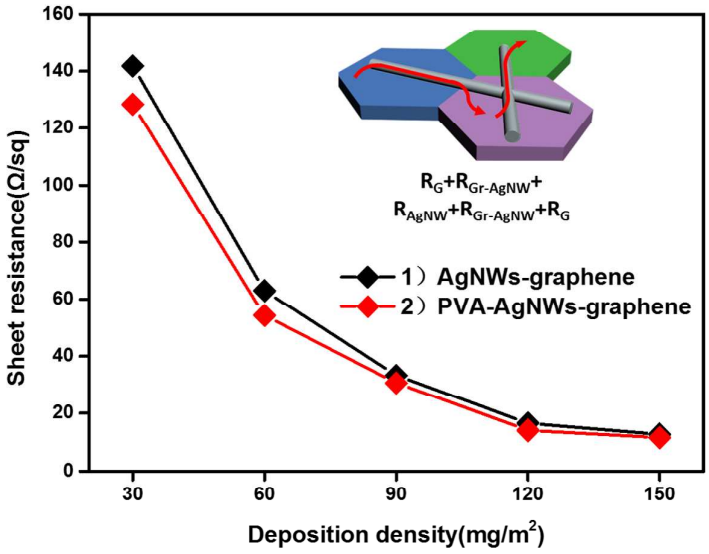

Fig. 3. Sheet resistance *vs* AgNWs deposition density of the AgNWs-graphene film and PVA encapsulated AgNWs-graphene hybrid film on PET substrate, the inset picture shows the available current flow paths.

the measured R_S of PVA encapsulated AgNWs-graphene hybrid films with the control pristine AgNWs-graphene hybrid films containing the same AgNWs density (curve 2), we find that there is further decrease in R_S, demonstrating the importance of PVA layer and the potential of our conductive electrode design. For example, a same increase in AgNWs deposition density from 30 to 150 mg/m^2 resulted in a larger decrease in R_S from 128.3 Ω/□ to 11.6 Ω/□ of AgNWs-graphene hybrid films with

coated PVA layer. We think that the reason why the R_S reduced after the hybrid film coated by PVA layer is that there exists an observable reduction in PVA thickness when it is dried after water evaporation as mentioned later, yielding a more intimate contact between AgNWs and graphene. As a result, $R_{\text{Graphene-AgNWs}}$ and $R_{\text{AgNWs-AgNWs}}$ was further reduced as shown in the inset of Figure 3.[24]

Figure 4a and 4b show the transmission spectra of the hybrid films before and after PVA treatments, respectively. Here the corresponding sample's plots of optical transmittance at 550nm were provided in Figure 4c and 4d with the purpose of creating a distinct contrast. It is seen that the increase of the AgNWs deposition density results in the decrease of the optical transmittance for both the pristine AgNWs-graphene hybrid films and AgNWs-graphene hybrid films with coated PVA layer. For the pristine AgNWs-graphene hybrid films, the optical transmittance decreases from 92.8% to 84.2% at 550 nm as the AgNWs deposition density is increased from 30 to 150 mg/m^2 (Figure 4a and 4c). After uniform spinning coating of PVA layer, the optical transmittance of the hybrid sample with the same AgNWs deposition density is slightly decreased, in which the optical transmittance of the hybrid film changes from 90.5% to 80.5% at 550nm as the AgNWs deposition density increases from 30 to 150 mg/m^2 (Figure 4b and 4d), the similar trend could be observed in the insets of real images of Figure 4d. The slightly decreased transparency of is primarily due to the introduction of the PVA layer which may shade a part of visible light. However, when the optical transmittance is around 84 % at 550 nm, here the R_S is only 14.1 Ω/□ for the PVA encapsulated AgNWs-graphene hybrid film,

which is superior to the conventional ITO and many other conductive materials as shown in Figure 5.[12,22,24,32] This also means that the positive effects of PVA layer are greater than the negative influences in the hybrid films.

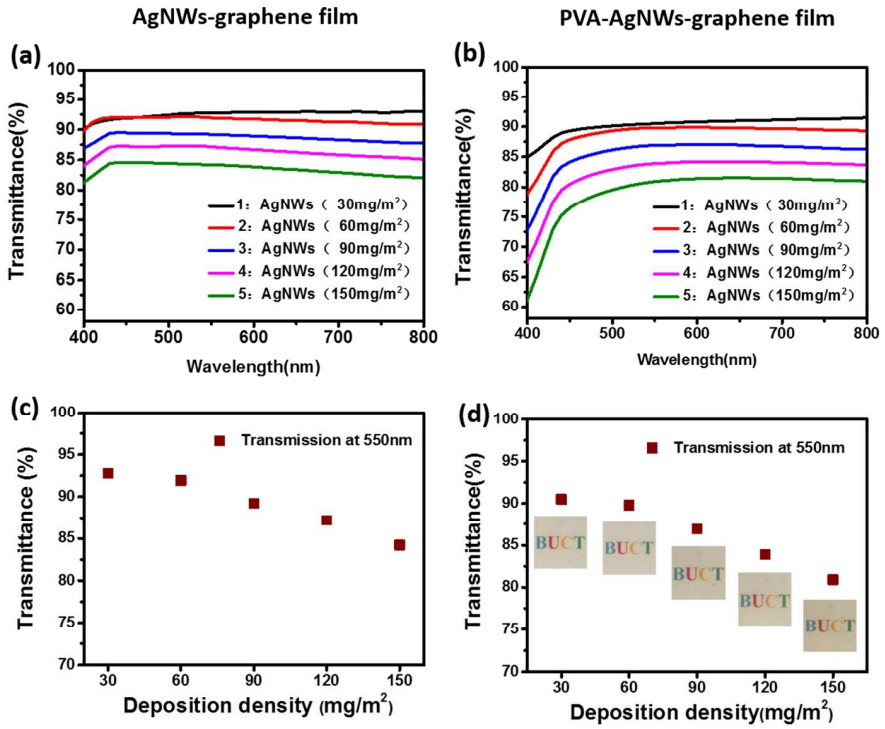

Fig. 4 (a)-(b): Optical transmittance spectra of AgNWs–graphene film and PVA encapsulated AgNWs-graphene hybrid film on PET substrate at different deposition densities; (c)-(d): Transmittance of AgNWs–graphene film and PVA encapsulated AgNWs-graphene hybrid film at 550nm at different deposition densities. The inset pictures are real images of PVA encapsulated AgNWs-graphene hybrid films on PET substrates with different deposition densities

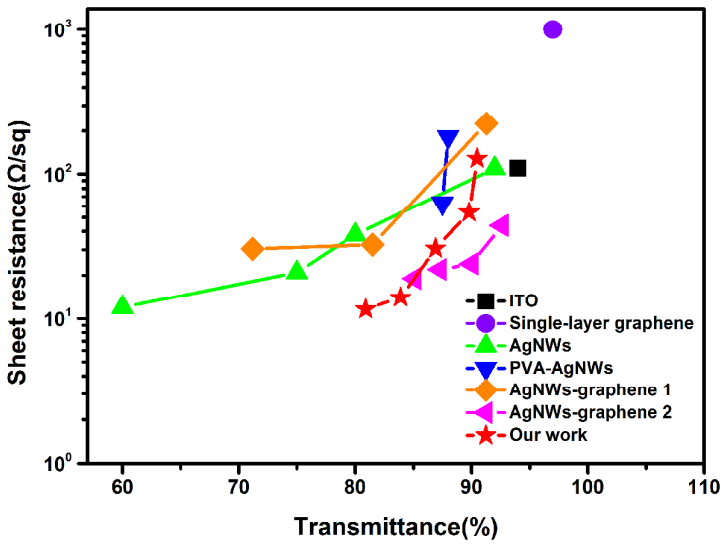

Fig. 5 Comparison of optical transmittance (at 550 nm) versus sheet resistance for our work and other conductive materials: ITO, single-layer graphene, AgNWs,[12] AgNWs-graphene[22,24] and PVA-AgNWs[32]

To obtain an understanding of the morphology of the hybrid films on the electrical and optical performances, the hybrid films are characterized by SEM. The left section of Figure 6a shows the SEM images of the pristine AgNWs-graphene hybrid films with different AgNWs deposition density. We can observe that, the AgNWs meshes become progressively intensive on the single-layer graphene film with an increase of the AgNWs deposition density from 30 to 150 mg/m^2, especially from the enlarged SEM images. As mentioned above, the increase AgNWs deposition density yields the improved electrical conductance of the AgNWs-graphene hybrid films, which is contributed to the increased electron transport channels by the added connections formed among the graphene-AgNWs and AgNWs-AgNWs as shown in the inset of

Figure 3.

In order to evaluate the influence of the PVA layer on the hybrid films we choose two samples, in which one is the pristine hybrid film containing AgNWs (deposition density is 120 mg/m^2) and single-layer graphene, and another sample consists of PVA-encapsulated AgNWs with the same deposition density and single-layer graphene. This needs to be stressed that these two samples were deposited upon the glass, so the samples of the cross-section SEM images can be handled easily. Herein, the PVA layer should have an appropriate thickness by controlling the fabrication parameters (spin-coated, 3000r, 60s), leading that AgNWs can be totally buried at the surface of PVA layer. Figure 6b-6c shows the SEM images of these two samples, by comparing with the pristine AgNWs-graphene hybrid film, we can see that the PVA-encapsulated AgNWs-graphene hybrid film looks a little obscure due to the existence of PVA layer, which demonstrates that PVA was assuredly covered upon the pristine hybrid film. This observation was further verified by the cross-section SEM images (the lower section of Figure 6b-c) of these two samples, it could be seen that the pristine AgNWs mesh was not continuous; while the hybrid film became flat and smooth after coating with PVA layer.

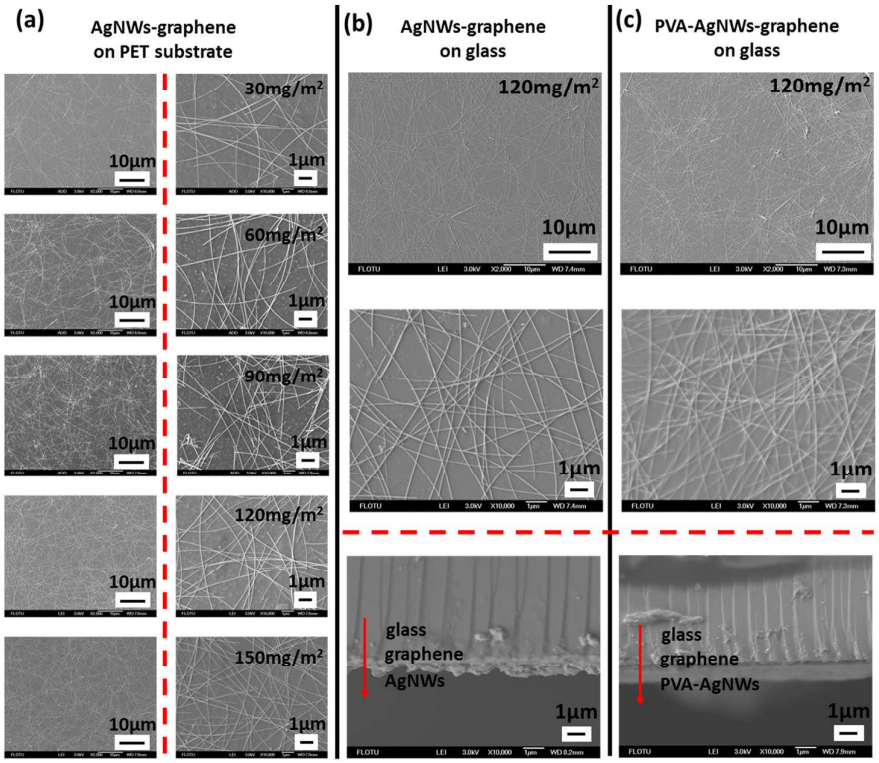

Fig. 6 (a): SEM images of the pristine AgNWs-graphene hybrid film on PET substrate. The AgNWs deposition density of the five samples increased from 30mg/m^2 to 150mg/m^2, each sample was imaged at two different magnifications. (b)-(c): The upper section shows the SEM images of AgNWs-graphene film and PVA encapsulated AgNWs-graphene hybrid film at two magnifications. The AgNWs deposition density of each sample was 120mg/m^2 and the AgNWs deposited on glass. The lower section shows the cross-section SEM images of each corresponding sample.

To further study the effect of PVA on the hybrid electrode, AFM images were taken and analyzed from the same two contrast samples, where these two samples were deposited on PET substrates. AFM images are shown in Figure 7a and 7a', for the pristine AgNWs-graphene hybrid film, the root mean square (RMS) roughness was

measured at 32.6 nm, which is not suitable with high-efficiency electronic devices. However, the surface roughness drops to around 6.36 nm after the hybrid film was encapsulated by PVA layer. Furthermore, from the Figure 7c-c', we can find that the rough surface turns to a flat plane when the AgNWs network was treated by PVA. Therefore, the surface roughness of the hybrid films can be decreased significantly by coated a PVA layer.

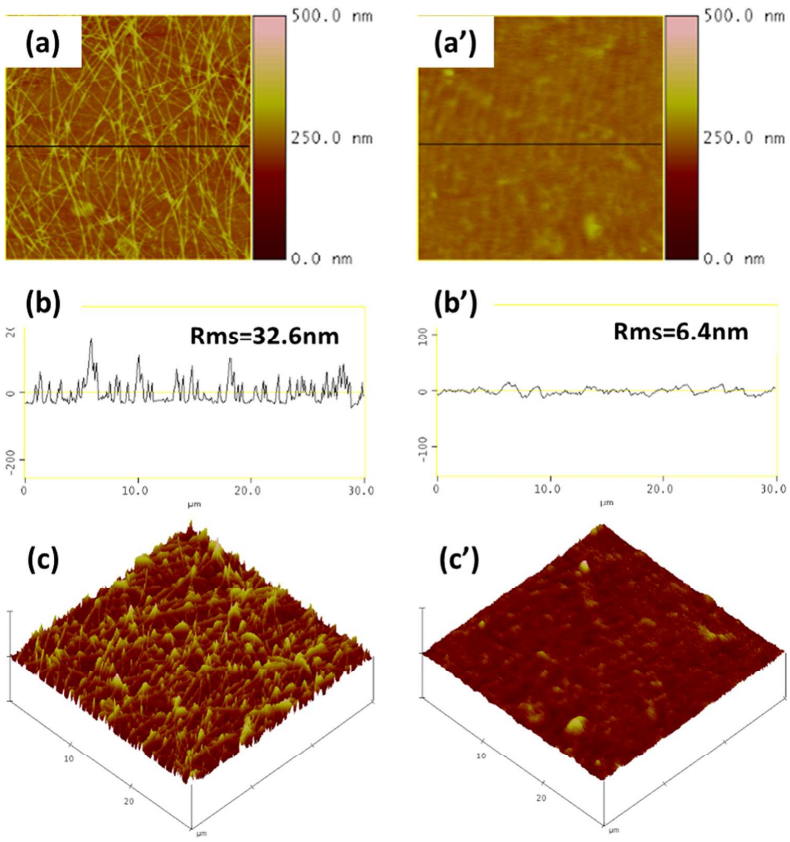

Fig. 7 (a)-(a'): AFM image of AgNWs-graphene film and PVA encapsulated AgNWs-graphene hybrid film on a PET substrate; (b)-(b'): Section curves and roughness of AgNWs-graphene film and PVA encapsulated AgNWs-graphene hybrid film on a PET substrate; (c)-(c'): 3D AFM image of AgNWs-graphene film and PVA encapsulated AgNWs-graphene hybrid film.

As is known that, mechanical flexibility is one of the most important parameters for the emerging optoelectronic devices application, such as flexible displays and solar cells. Therefore, we further estimate the mechanical robustness against bending of the hybrid films. Herein, in order to get an effect comparisons between the hybrid films and ITO on PET substrate, we prepared a PVA encapsulated AgNWs-graphene hybrid film (Rs= 109.2 Ω/□, 30 mm×30 mm) and the corresponding the pristine AgNWs-graphene hybrid film (Rs= 114.6 Ω/□, 30 mm×30 mm) on PET substrates, which have similar R_S with ITO on PET substrate (Rs= 105.2 Ω/□, 30 mm×30 mm). Figure 8 shows the R_S as a function of bending time curve, in this measurement, these three samples are rolled around a bending radius of 5 mm, and the R_S of each sample is compared to its initial value. Within the few cycles of this process, the ITO film begins to crack, yielding a sharp increase in R_S (curve 1, Figure 8), which is due to that the inherently brittleness of ITO. On the contrary, as shown in Figure 8, the R_S of PVA encapsulated AgNWs-graphene hybrid changed little after thousands of bending (curve 2), whereas R_S of the pristine AgNWs-graphene hybrid film increased to more than 300% (curve 3). The mechanical robustness of PVA encapsulated AgNWs-graphene hybrid film may be contributed to the formation of well-constructed electron transfer networks encapsulated by PVA layer in the hybrid film, thereby exhibiting a high tolerance to bending and excellent mechanical stability.

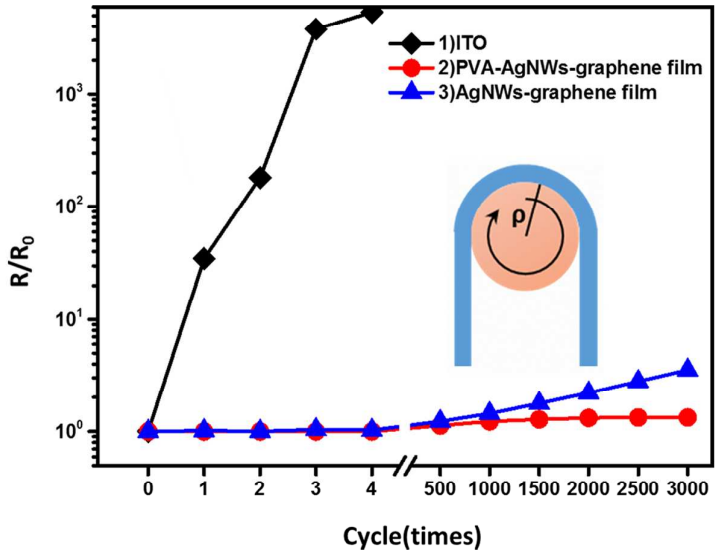

Fig. 8 R_S/R_0 vs cycle of bends for the ITO, AgNWs-graphene film and PVA encapsulated AgNWs-graphene hybrid film on PET substrate, the inset picture shows the typical bending process.

To determine the effect of the PVA layer on the chemical stability of the hybrid films we choose another two hybrid films as the object of study, where one is PVA encapsulated AgNWs-graphene hybrid film with 120 mg/m^2 AgNWs deposition density (Sample 1, R_S=15.1 Ω/□) and another is pristine AgNWs-graphene hybrid film (sample 2, R_S=18.2 Ω/□) as a reference sample. Both of them were exposed in high temperature (80 ^oC) and high humidity (50% RH) conditions for 7 days, and we record the R_S of these two samples for every 24 hours. As shown in Figure 9, we can observe that the R_S of sample 2 of the pristine AgNWs-graphene hybrid film notably increased (curve 1, Figure 9), which is due to that large surface area of the AgNWs was exposed to air, resulting that the relatively ease of oxidation. When the AgNWs are oxidized, the electrical resistivity and junction resistance of the AgNWs would

increase because of the formation of silver oxides on the surface of the AgNWs. By comparing the sample 1 with this reference sample 2, we find that there is almost no degradation of R_S after the thermal oxidation stability testing, the R_S of sample 2 slightly increased less than 15% even after 7 days (curve 2, Figure 9). This striking difference in change of R_S between the sample 1 and sample 2 clearly verifies that the AgNWs encapsulated by PVA layer can effectively prevent air oxidation in the air and has a perfect chemical stability. Therefore, the existence of PVA layer is one of the vital factors determining the stability of conductivity in the hybrid film.

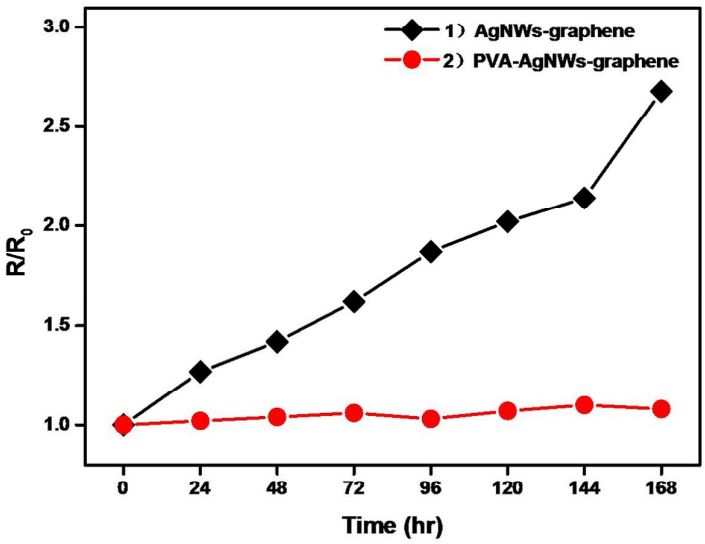

Fig. 9 Sheet resistance change of AgNWs-graphene hybrid film and PVA encapsulated AgNWs-graphene hybrid film on PET substrate during the long-term stability test at 80°C and 50% RH for 7 days.

To verify the performance of the PVA encapsulated AgNWs-graphene hybrid film as an electrode for flexible display, here we employ this hybrid electrode film to build a photo-addressed/electric-erased flexible Ch-LCs device. In this proof-of-concept

device, the Ch-LCs mixture was laminated between two PVA encapsulated AgNWs-graphene hybrid film on PET substrates as the bottom and top electrodes as shown in Figure 10a. It is worthy of noting that, the PVA layer after mechanical rubbing in this hybrid electrode film was also used as an orientation layer to induce a planar alignment for Ch-LCs molecules. Figure 10b-e shows the images of the LC device at different states, the flexible Ch-LCs device exhibits a blue reflection color at an initial planar state as shown in Figure 10b, and a "BUCT" pattern was addressed on the LC cell by using UV light with a negative photomask placed on the top of the cell (Figure 10c). When the intensity of electric (E)-field reaches to 22.1V, the patterned image can be completely erased (Figure 10d) due to the formation of weak scattering state of Ch-LCs molecules. Finally, the reflective image "BUCT" can reappear when a 51.5 V E-field pulse was applied to the LC cell (Figure 10e). A reversibly and dynamically switching process between the above two states by controlling the applied voltage was also provided in a video file (see SI, Movie 1). Our experimental results demonstrate that, compared with the previous ITO-based Ch-LCs device, there is no observable degradation in performance in this ITO-free device under our experimental conditions. Most important thing is that, this LC device could be bended and still exhibits a high resolution image (Figure 10f), demonstrating that this kind of hybrid electrode film has a great potential for flexible devices.

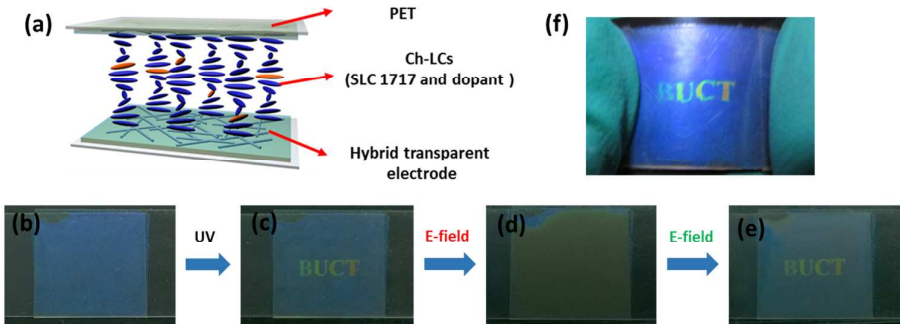

Fig. 10 (a): Schematic diagram of Ch-LCs device; (b-e): Real LC cell images of this flexible, photo-addressed/electric-erased and multi-switchable Ch-LCs device at different states; (f): A flexible show for this LC device.

Conclusions

In summary, we fabricated a highly stable and flexible hybrid electrode composed of single-layer graphene and silver nanowire network embedded by PVA layer on PET substrate. Compared with ITO and the control AgNWs-graphene hybrid electrode film, the PVA encapsulated AgNWs-graphene hybrid films exhibit improved electrical and considerable optical performances. Meanwhile, the hybrid electrode films show highly antioxidation and mechanical flexibility due to the PVA layer acts as a protection layer. Furthermore, a photo-addressed/electric-erased flexible Ch-LCs device on PET substrate was constructed by laminating the Ch-LCs mixture between these two hybrid electrodes. The fabricated flexible LC device exhibits a desired switching performance with a more stretchable performance. This work shows a potential approach to improving the overall performances of AgNWs-graphene hybrid electrodes by introducing multi-functional polymers, such as PVA, polyimide and even biodegradable polymer adhesives.

Acknowledgments

This research was supported by the National Natural Science foundation (Grant no. 51373013, 51173013 and 50903004) and Beijing Young Talents Plan (YETP0489).

References

1 D. S. Hecht, L. Hu and G. Irvin, *Adv. Mater.*, 2011, **23**, 1482-1513.

2 D. S. Hecht and R. B. Kaner, *MRS Bull.*, 2011, **36**, 749-755.

3 S. Kirchmeyer and K. Reuter, *J. Mater. Chem.*, 2005, **15**, 2077-2088.

4 A. G. MacDiarmid, *Angew. Chem. Int. Ed.*, 2001, **40**, 2581-2590.

5 Z. Wu, Z. Chen, X. Du, J. M. Logan, J. Sippel, M. Nikolou, K. Kamaras, J. R. Reynolds, D. B. Tanner, A. F. Hebard and A. G. Rinzler, *Science*, 2004, **305**, 1273-1276.

6 E. M. Doherty, S. De, P. E. Lyons, A. Shmeliov, P. N. Nirmalraj, V. Scardaci, J. Joimel, W. J. Blau, J. J. Boland and J. N. Coleman, *Carbon*, 2009, **47**, 2466-2473.

7 X. Li, Y. Zhu, W. Cai, M. Borysiak, B. Han, D. Chen, R. D. Piner, L. Colombo and R. S. Ruoff, *Nano Lett.*, 2009, **9**, 4359-4363.

8 M.-G. Kang, M.-S. Kim, J. Kim and L. J. Guo, *Adv. Mater.*, 2008, **20**, 4408-4413.

9 H. Wu, L. Hu, M. W. Rowell, D. Kong, J. J. Cha, J. R. McDonough, J. Zhu, Y. Yang, M. D. McGehee and Y. Cui, *Nano Lett.*, 2010, **10**, 4242-4248.

10 S. De, T. M. Higgins, P. E. Lyons, E. M. Doherty, P. N. Nirmalraj, W. J. Blau, J. J. Boland and J. N. Coleman, *ACS Nano*, 2009, **3**, 1767-1774.

11 S. De, P. J. King, P. E. Lyons, U. Khan and J. N. Coleman, *ACS Nano*, 2010, **4**, 7064-7072.

12 L. Hu, H. S. Kim, J.-Y. Lee, P. Peumans and Y. Cui, *ACS Nano*, 2010, **4**, 2955-2963.

13 A. B. Kuzmenko, E. van Heumen, F. Carbone and D. van der Marel, *Phys. Rev. Lett.*, 2008, **100**, 117401(1)-(4).

14 S. Pang, Y. Hernandez, X. Feng and K. Mullen, *Adv. Mater.*, 2011, **23**, 2779-2795.

15 S. Bae, H. Kim, Y. Lee, X. Xu, J.-S. Park, Y. Zheng, J. Balakrishnan, T. Lei, H. Ri Kim, Y. I. Song, Y.-J. Kim, K. S. Kim, B. Ozyilmaz, J.-H. Ahn, B. H. Hong and S. Iijima, *Nat. Nanotechnol.*, 2010, **5**, 574-578.

16 Y. Lee, S. Bae, H. Jang, S. Jang, S.-E. Zhu, S. H. Sim, Y. I. Song, B. H. Hong and J.-H. Ahn, *Nano Lett.*, 2010, **10**, 490-493.

17 H. Cao, Q. Yu, L. A. Jauregui, J. Tian, W. Wu, Z. Liu, R. Jalilian, D. K. Benjamin, Z. Jiang, J. Bao, S. S. Pei and Y. P. Chen, *Appl. Phys. Lett.*, 2010, **96**, 122106(1)-(3).

18 J. Guo, C. M. Huard, Y. Yang, Y. J. Shin, K.-T. Lee and L. J. Guo, *Adv. Opti. Mater.*, 2014, **2**, 435-441.

19 I. N. Kholmanov, C. W. Magnuson, A. E. Aliev, H. Li, B. Zhang, J. W. Suk, L. L. Zhang, E. Peng, S. H. Mousavi, A. B. Khanikaev, R. Piner, G. Shvets and R. S. Ruoff, *Nano Lett.*, 2012, **12**, 5679-5683.

20 B. H. Lee, J.-H. Lee, Y. H. Kahng, N. Kim, Y. J. Kim, J. Lee, T. Lee and K. Lee, *Adv. Funct. Mater.*, 2014, **24**, 1847-1856.

21 C. Jeong, P. Nair, M. Khan, M. Lundstrom and M. A. Alam, *Nano Lett.*, 2011, **11**, 5020-5025.

22 Y. Liu, Q. Chang and L. Huang, *J. Mater. Chem. C*, 2013, **1**, 2970-2974.

23 D. L. H. L. Y. A. Y. J. D.-Y. L. Y. Lee, *Nanoscale*, 2013, **5**, 7750-7755.

24 R. Chen, S. R. Das, C. Jeong, M. R. Khan, D. B. Janes and M. A. Alam, *Adv. Funct. Mater.*, 2013, **23**, 5150–5158.

25 M. S. Lee, K. Lee, S. Y. Kim, H. Lee, J. Park, K. H. Choi, H. K. Kim, D. G. Kim, D. Y. Lee, S. Nam and J. U. Park, *Nano. Lett.*, 2013, **13**, 2814-2821.

26 T. Kim, Y. W. Kim, H. S. Lee, H. Kim, W. S. Yang and K. S. Suh, *Adv. Funct. Mater.*, 2013, **23**, 1250-1255.

27 J. Lee, P. Lee, H. B. Lee, S. Hong, I. Lee, J. Yeo, S. S. Lee, T.-S. Kim, D. Lee and S. H. Ko, *Adv. Funct. Mater.*, 2013, **34**, 4171–4176.

28 Z. Yu, Q. Zhang, L. Li, Q. Chen, X. Niu, J. Liu and Q. Pei, *Adv. Mater.*, 2011, **23**, 664-668.

29 J.-Y. Lee, S. T. Connor, Y. Cui and P. Peumans, *Nano Lett*., 2008, **8**, 689-692.

30 W. Gaynor, G. F. Burkhard, M. D. McGehee and P. Peumans, *Adv. Mater.*, 2011, **23**, 2905-2910.

31 S. M. I. Al-Rafia and J. M. Buriak, *ACS Appl. Mat. Interfaces*, 2013, **5**, 12663-12671.

32 X. Y. Zeng, Q. K. Zhang, R. M. Yu and C. Z. Lu, *Adv. Mater.*, 2010, **22**, 4484-4488.

33 T. Akter and W. S. Kim, *ACS Appl. Mat. Interfaces*, 2012, **4**, 1855-1859.

34 Z. Yu, L. Li, Q. Zhang, W. Hu and Q. Pei, *Adv. Mater.*, 2011, **23**, 4453-4457.

35 Y. Xie, D. Fu, O. Jin, H. Zhang, J. Wei and J. Guo, *J. Mater. Chem. C*, 2013, **1**, 7346-7356.

Graphic Abstract:

Table of contents entry

Text:

High-stable and flexible graphene-polymer processed silver nanowires hybrid transparent electrodes and their application for flexible liquid crystal display were demonstrated.

Color graphic: